WITHDRAWN: Nitrogen-Doped Carbon Boosting Fe_2O_3 Anode Performance for Long-Life Supercapacitors

kaijie dong
Jiangnan University
zhaokun yang
Jiangnan University
dongjian shi
Jiangnan University
Mingqing Chen
mqchen@jiangnan.edu.cn
Jiangnan University
weifu dong
Jiangnan University

Research Article

Keywords: Fe2O3, Polyaniline, N-doped porous carbon, in situ growth, supercapacitor

Posted Date: November 30th, 2021

DOI: https://doi.org/10.21203/rs.3.rs-1113132/v1

EDITORIAL NOTE:

The full text of this preprint has been withdrawn by the authors while they make corrections to the work. Therefore, the authors do not wish this work to be cited as a reference. Questions should be directed to the corresponding author.

Abstract

Here, we report Fe_2O_3/N-doped carbon (Fe_2O_3/CN) composites via one-step facile calcination process by using FeOOH and PANI as precursor. The results show that N-doped carbon is helpful to enhance the electrochemical properties of Fe_2O_3. N-doped carbon not only enhances the conductivity of Fe_2O_3 electrode, but also alleviates the volume expansion of Fe_2O_3 in the process of repeated charge and discharge. In addition, the synergistic effect of Fe_2O_3 and N-doped porous carbon makes the composites show higher capacitive properties (538.7 mF/cm^2 at 5 mA/cm^2) and cycle life (100% retention after 2000 cycles). In addition, its superior electrochemical performance is also proved in symmetrical supercapacitor. After 4900 cycles with current density of 10 mA/cm^2, its capacity retention rate is 100%. So Fe_2O_3/N-doped carbon as electrode materials for long-life symmetrical supercapacitors has broad application prospects.

1. Introduction

Compared with other energy storage devices (such as Lithium-ion battery, Sodium ion battery, Zinc ion battery e.g.), chemical capacitors, also known as supercapacitors, have the advantages of high-power density, fast charge and discharge speed and long cycle life [1, 2, 3, 4]. However, the relatively low energy density of supercapacitors still hinders their large-scale practical application [5, 6, 7]. It is very necessary to develop advanced supercapacitors with the comprehensive advantages of high energy density [8, 9, 10]. According to the energy density formula the energy density is proportional to the specific capacitance and voltage of the supercapacitor. The specific capacitance of supercapacitor is closely related to the performance of electrode material [11, 12, 13]. Compared with the reported positive materials, the specific capacitance of negative materials is often unsatisfactory. In order to construct high performance supercapacitors, it is urgent to develop negative materials with high capacity and high cycle stability. [14].

Among the negative electrode materials, Fe_2O_3 has been widely studied because of its low price, high theoretical capacity, natural abundance and non-toxicity [15, 16, 17, 18, 19, 20, 21]. Nevertheless, there are still some problems in the process of constant current charge and discharge, such as poor conductivity and large volume change, resulting in serious electrode pulverization, particle cracking and capacity loss [22, 23]. In order to overcome these problems, various strategies have been developed, such as surface coating with conductive materials and constructing nanostructured materials with different morphologies [24, 25, 26, 27, 28]. Among these methods, the design of Fe_2O_3/carbon composites with nano structure shows great application prospects in commercial applications because of their economical preparation methods [29]. Specifically, as a unique protective coating, carbon has been widely used in electrode materials because of its excellent electronic conductivity, chemical stability and large surface area [30, 31]. The research shows that Fe_2O_3/carbon composites not only improve the conductivity of Fe_2O_3, but also enhance the electrochemical properties of Fe_2O_3. For example, carbon coated Fe_2O_3 nanorods on carbon fiber have recently been reported and exhibit a specific capacity of 384.3 mAh/g at a current density of 2 A/g [32]. In order to further improve the high-rate performance and long cycle stability of

Fe_2O_3/carbon composites, the modification of carbon materials is also a feasible and effective strategy. Doping of some heteroatoms (nitrogen (N), sulfur (S), phosphorus (P) and boron (B) can introduce more defects, disordered structures and more active sites, so as to improve the electrochemical performance [33, 34]. Although some studies on the application of Fe_2O_3/heteroatom doped carbon composites in supercapacitors have been reported, the electrochemical properties are not satisfactory.

Here, Fe_2O_3/N-doped carbon composites (Fe_2O_3/CN) are successfully prepared by one-step calcination process with FeOOH and polyaniline (PANI) as precursors. N-doped carbon improves the conductivity of the whole composite, so as to improve the cycle stability. The N-doped carbon layer provides a protective shell to adapt to the volume change of Fe_2O_3 during charge and discharge, which leads to the improvement of the stability of the whole electrode. The results show that Fe_2O_3/CN has better electrochemical properties than pure Fe_2O_3. Fe_2O_3/CN has excellent rate performance (e.g., 538.75 mF/cm^2 at 5 mA/cm^2 and 360 mF/cm^2 at 20 mA/cm^2) and excellent cycle performance (capacity retention rate of 100% after 2000 cycles at 25 mA/cm^2). In addition, we also construct a symmetrical supercapacitor with a capacity retention rate of 100% after 4900 cycles at 10 mA/cm^2. These promising results show that Fe_2O_3/CN can be used as ideal electrode materials for high magnification and long-life supercapacitor.

2. Materials And Methods

2.1. Preparation of Fe_2O_3/N-doped carbon (Fe_2O_3/CN).

The Fe_2O_3/CN electrode was manufactured by the following steps [35, 36]. Firstly, FeOOH was grown directly on carbon cloth substrate by hydrothermal method, and polyaniline was grown on FeOOH in situ. Specifically, 0.54 g of ferric chloride hexahydrate ($FeCl_3 \cdot 6H_2O$) and 0.284 g of sodium sulfate (Na_2SO_4) were dissolved in 40 ml of deionized water under magnetic stirring. The prepared aqueous solution was transferred to a 100 mL hydrothermal autoclave, in which four hydrophilic treated carbon cloths (1cm× 2cm) were fixed. Then, the autoclave was heated to 120°C and maintained for 7 h. After cooling to room temperature, the obtained carbon clothes were washed with deionized water to remove impurities.

Secondly, soak the dried carbon cloth in 0.01 mol/L aniline solution (0.1 mol/L phytic acid), and then add 0.6 mol/L ammonium persulfate solution to initiate polymerization. Subsequently, transferring the carbon cloth to a refrigerator at 3 ℃ for 8 h. After the reaction, the obtained product was washed three times with ethanol and deionized water and dried overnight at 60°C. Finally, the obtained carbon cloth was annealed in nitrogen at 400°C for 2 h.

2.2. Characterization

The morphology and structure of the products were examined by scanning electron microscopy (SEM, Hitachi s-4800, accelerating voltage of 5 kV, Japan). The phase composition of the sample was determined by X-ray diffraction (XRD) at 2 θ = Identification shall be carried out in the range of 10-70°.

The electronic states of the samples were studied by X-ray photoelectron spectroscopy (XPS, Phi 5000 versa probe). Its electrochemical properties were studied on ChI 660E electrochemical workstation (Chenhua ChI 660E). Fe_2O_3 and Fe_2O_3/CN are directly used as working electrodes on carbon fiber cloth.

2.3. Electrochemical measurements

The electrochemical test was evaluated by a standard three electrode system in 2.0 mol/L KOH aqueous solution. Platinum foil electrode is used as counter electrode. The Hg/HgO electrode was used as the reference electrode. Cyclic voltammetry (CV), electrochemical impedance spectroscopy (EIS) and chronopotentiometry (GCD) measurements were performed on the ChI660E electrochemical workstation to determine the electrochemical performance. The EIS is performed in the frequency range of 0.01 Hz and 100 kHz.

2.4. Fabrication of symmetric supercapacitor.

Symmetrical supercapacitor consists of Fe_2O_3/CN electrode. The electrolyte is 2.0 mol/L KOH aqueous solution. The whole device was tested in a standard double electrode system.

The specific capacitance (C, mF/cm^2), energy density (E, mWh/cm^2) and power density (P, mW/cm^2) are calculated by the following equation,

$$C=\frac{I\times\Delta t}{S\times\Delta V} \quad (1)$$

Where I is the constant current during the GCD discharge process, S is the area of active material on the working electrode, Δt is the discharge time during the GCD discharge process, and ΔV is the voltage change during the GCD discharge process.

$$V=\frac{C\times\Delta V^2}{2\times3600} \quad (2)$$

$$P=\frac{E}{\Delta t} \quad (3)$$

3. Results And Discussion

Fe_2O_3/CN was successfully synthesized on carbon cloth by hydrothermal, in-situ growth and calcination, and the synthesis process is shown in Scheme 1. In short, macro woven carbon cloth with good flexibility and conductivity is used as the support of composite structure. Precursors are formed on the surface of carbon cloth by hydrothermal and in-situ synthesis. Fe_2O_3/CN composites are synthesized by one-step

calcination, including loaded Fe_2O_3 nanorod arrays and N-doped carbon coatings to ensure effective electrolyte penetration and further inhibit the pulverization of active substances.

The morphologies of Fe_2O_3 and Fe_2O_3/CN are firstly examined by SEM. As shown in Fig. 1a and c, Fe_2O_3 nanorods are uniformly and densely covered with carbon cloth, with a diameter of 100 nm and clear two-dimensional characteristics (Fig. 1c). SEM images (Fig. 1b, d) show that the N-doped carbon layer has many pores, and the N-doped carbon is attached to Fe_2O_3 nanorods. The SEM image of magnification shows that N-doped carbon is stacked by many nano rods with a diameter of 50-100 nm, which is the reason for the porosity of N-doped carbon layer (Fig. 1d). In addition, the presence of N-doped carbon alleviates the mechanical stress caused by the volume expansion of Fe_2O_3, and reduces the powder damage during Fe_2O_3 charge and discharge.

The crystal structure of Fe_2O_3 and its composites are confirmed by XRD, and XRD pattern of carbon cloth, Fe_2O_3 and Fe_2O_3/CN is shown in Fig. 3a. Obviously, after calcination in nitrogen, diffraction peaks at 24°, 33°, 35° and 49° in Fe_2O_3 and Fe_2O_3/CN are consistent with hematite (JCPDS No. 33-0664), indicating that the Fe_2O_3 nanorods on carbon cloth are successfully synthesized [37]. And no impurity peak is observed in the whole pattern, indicating the high purity of the final product. It is worth noting that the peak of Fe_2O_3/CN becomes stronger and sharper, indicating a slight increase in crystallinity. Fig. 3b shows Raman spectra to characterize the structure and surface chemistry of Fe_2O_3 and Fe_2O_3/CN. In the two samples, typical Raman peaks of Fe_2O_3 can be clearly distinguished, which are concentrated near 218, 279, 391 and 1330 cm^{-1}, indicating that Fe_2O_3 is loaded on the carbon cloth [38]. This is consistent with the analysis results of XRD pattern. In addition, the detection of the D band at 1315 cm^{-1} and the G band at 1603 cm^{-1} in Raman spectrum of Fe_2O_3/CN is attributed to disordered Sp^3 hybrid carbon (A_{1g} symmetry) and graphite Sp^2 hybrid carbon (E_{2g} symmetry, respectively) [39]. This indicates that Fe_2O_3/CN is successfully prepared. The I_D/I_G of Fe_2O_3 is 1.2, indicating that the disorder caused by the surface of carbon fiber is high. The I_D/I_G of Fe_2O_3/CN is 1.05, which is lower than that of carbon fiber, showing a higher degree of graphitization, because the carbon crystallinity of polyaniline after annealing is high in nitrogen [40]. The phenomenon is consistent with the test results of XRD.

In order to check the surface chemical composition and oxidation valence state of all samples, XPS measurements are carried out. From the full spectrum, the sample shows the signals of O, Fe, N and C from Fe_2O_3/CN. The emerging of N element is attributed to N-doped carbon on the surface of Fe_2O_3. As shown in the O 1s spectrum of Fe_2O_3/CN, the peaks at 534.8, 531.5 and 530.1 eV belong to O-H, C-O and Fe-O, respectively [41]. The illustration in Fig. 3c shows the high-resolution spectrum of the Fe 2p region, indicating that Fe 2p is composed of Fe $2p_{3/2}$ and Fe $2p_{1/2}$, corresponding to the binding energies of 711.2 and 724.8 eV, respectively [42]. Between the peaks of Fe $2p_{3/2}$ and Fe $2p_{1/2}$, the satellite peak of 718.8 eV can explain the pure trivalent property. The result corresponds to the crystal structure of Fe_2O_3 in XRD. In the C 1s spectrum, the three peaks can be attributed to C-N (288.8 eV), C-O (285.9 eV) and C-C (284.7 eV), respectively, which proves that N atoms are successfully doped in carbon materials (Fig. 3d)

[43]. In addition, the N 1s spectrum can be fitted into two peaks (Fig. S1). The first peak at 398.5 eV corresponds to pyridine-N [44]. The second peak at 400.3 eV belongs to graphite-N. Pyridine-N provides redox active sites for additional pseudo capacitance, while graphite nitrogen reduces the charge transfer resistance due to the enhancement of conductivity. Therefore, Fe_2O_3/CN is successfully prepared, which is consistent with the results of Raman spectrum XRD and SEM.

The prepared electrodes used a three-electrode system to evaluate their electrochemical properties in 2 mol/L KOH electrolyte. The electrochemical properties of Fe_2O_3 and Fe_2O_3/CN electrodes are studied by cyclic voltammetry (CV), galvanostatic charge discharge (GCD) and electrochemical impedance spectroscopy (EIS). Fig. 4a shows the comparative CV curves of Fe_2O_3 and Fe_2O_3/CN recorded at 100 mV/s. (see Fig. S3, supporting information for the CV curves of Fe_2O_3 and Fe_2O_3/CN electrode material at different scan rates). Fe_2O_3/CN electrode showed a better performance than the Fe_2O_3 electrode. The large CV curve area of Fe_2O_3/CN shows that the capacitance behavior is greatly enhanced due to the synergistic effect of CN electric double layer and Fe_2O_3 pseudo capacitor characteristics. The CV curve has a similar quasi moment shape, which further shows that Fe_2O_3/CN is charged/discharged at a pseudo constant rate throughout the voltammetric cycle, accompanied by a rapid faraday reaction between basic cations [30, 31, 32]. This phenomenon is due to the increase of capacitance caused by the enhancement of the conductivity of the whole electrode material by N-doped carbon. Fig. 3b shows the GCD curves of Fe_2O_3 and Fe_2O_3/CN electrodes at 15 mA/cm^2 current density. The longer the discharge time of Fe_2O_3/CN electrode, it shows that it has higher capacitance than Fe_2O_3 electrode, which is consistent with CV results. This is attributed to the fact that the presence of N-doped carbon promotes the improvement of the capacitance of iron oxide [45]. The conductivity enhancement of Fe_2O_3 is consistent with the above CV curve analysis. This phenomenon shows that N-doped carbon improves the capacitance of Fe_2O_3, reduces the interfacial internal resistance between Fe_2O_3 and N-doped carbon, and provides more active sites [46].

As shown in Fig. 4c, the EIS data of Fe_2O_3 and Fe_2O_3/CN electrodes show that the charge transfer resistance of Fe_2O_3/CN is less than that of bare Fe_2O_3 electrode shows that the addition of N-doped carbon layer leads to the enhancement of the conductivity of Fe_2O_3/CN electrode. Fe_2O_3/CN electrode has a more ideal straight line and low Warburg resistance, resulting in the rapid transfer of electrolyte ions to the hybrid electrode [47]. Fig. 4d shows the calculation results of specific capacitance of Fe_2O_3 and Fe_2O_3/CN electrodes with different current densities. Compared with the value of bare Fe_2O_3 electrode at current density of 5 mA/cm^2, the maximum specific capacitance of Fe_2O_3/CN electrode is 538.7 mF/cm^2, showing greater capacitance characteristics. The result suggests that N-doped carbon could efficaciously enhance the capacitance characteristics of Fe_2O_3, which could be attributed to the enhanced conductivity of Fe_2O_3/CN electrode.

Figure S2 shows the cyclic stability of Fe_2O_3/CN and Fe_2O_3. In the initial cycle, the charge transfer resistance (R_{ct}) decreases due to the activation of the electrode, so the electrode capacity increases. It is

worth noting that after 2000 cycles at a high current density of 25 mA/cm^2, the capacitance retention is 100% (Figure S2), which is higher than that of bare metal Fe_2O_3 electrode. These results confirm the effectiveness of our strategy. The performance of Fe_2O_3 electrode is greatly improved by surface N-doping carbon.

In order to further evaluate the possibility of Fe_2O_3/CN electrode material in practical energy storage application, a symmetrical supercapacitor is assembled with Fe_2O_3/CN as cathode and anode, and tested in 2 mol/L KOH electrolyte. Fig. 5a shows the CV curves recorded by the Fe_2O_3/CN//Fe_2O_3/CN symmetrical supercapacitor device at different scanning rates of 10 to 200 mV/s in the 0-1.0 V voltage window. All CV curves are quasi rectangular and highly symmetrical, reflecting good reversibility and typical capacitance behavior. As shown in Fig. 5b, the symmetrical GCD curve with excellent coulomb efficiency and triangular shape further proves that the symmetrical supercapacitor device we assembled has excellent energy storage performance. The Fe_2O_3/CN//Fe_2O_3/CN symmetric supercapacitor devices show good cyclic performance. Fig. S4 shows that after 4900 cycles at a high current density of 10 mA/cm^2, the capacitance retention is 100%. In addition, we further calculate the energy density and power density of the equipment, and the results are shown in Fig. 5d.

It is impressive that Fe_2O_3/CN//Fe_2O_3/CN symmetric supercapacitor devices can achieve an energy density of 0.011 mWh/cm^2 at a power density of 0.4 mW/cm^2, and can still maintain an energy density of 4 mWh/cm^2 at a power density of 0.0062 mW/cm^2. Although the device performance may be different due to electrode material preparation methods and electrochemical test conditions, under similar test conditions, our device performance is better than most reported supercapacitor devices.

Based on these results, Fe_2O_3/CN//Fe_2O_3/CN symmetric supercapacitor device shows excellent electrochemical behavior, which is attributed to the synergy between the components. As a powerful protective shell, N-doped carbon plays an extremely important role in the volume change of Fe_2O_3, which can prevent the corrosion and stress deformation of active materials. N-doped carbon can improve the conductivity of Fe_2O_3/CN electrode, effectively improve the stability of active material in long-term cycle and improve the capacitance of active material. In addition, the N-doped carbon loaded on Fe_2O_3 array has a unique pore structure and retains the channel for electrolyte ions to quickly approach the electrode surface. Therefore, Fe_2O_3/CN//Fe_2O_3/CN symmetric supercapacitor devices have excellent capacitance characteristics and is an attractive candidate material in commercial energy storage equipment.

4. Conclusion

In short, Fe_2O_3/CN electrodes are fabricated using a simple one-step calcination route. Compared with Fe_2O_3 (447.5 mF/cm^2), the Specific capacitance value of Fe_2O_3/CN electrode increases by 538.7 mF/cm^2. The results show that the presence of N-doped carbon makes Fe_2O_3/CN electrode have excellent capacitance and long-term cycle stability (a capacitance retention of 100% after 2000 cycles at

a high current density of 25 mA/cm^2). In addition, the assembled Fe_2O_3/CN//Fe_2O_3/CN symmetric supercapacitor device provides a maximum energy density of 0.011 mWh/cm^2 at a power density of 0.4 mW/cm^2, and can still maintain an energy density of 4 mWh/cm^2 at a power density of 0.0062 mW/cm^2. In addition, it also has an excellent capacity retention of 100% of the original capacitance after 4900 cycles at a high current density of 10 mA/cm^2. This study provides a feasible method for assembling Fe_2O_3/CN//Fe_2O_3/CN symmetric supercapacitor device with excellent electrochemical properties as the next generation of energy storage equipment.

Declarations

Acknowledgments

This work was partly supported by the National Nature Science Foundation of China (grant number 21571084), the Natural Science Foundation of Jiangsu Province (grants number BK20181349), National First-Class Discipline Program of Light Industry Technology and Engineering (grants number LIFE2018-19) and MOE & SAFEA for the 111 Project (grants number B13025).

References

1. H.P. Feng, L. Tang, G.M. Zeng, J. Tang, Y.C. Deng, M. Yan, Y.N. Liu, Y.Y. Zhou, X.Y. Ren, S. Chen, Carbon-based core–shell nanostructured materials for electrochemical energy storage. J. Mater. Chem. A **6**, 7310–7337 (2018)
2. L. Peng, Z. Fang, Y. Zhu, C. Yan, G. Yu, Holey 2D Nanomaterials for Electrochemical Energy Storage. Adv. Energy Mater. **8**, 1702179 (2017)
3. H. Yu, Y. Wang, Y. Jing, J. Ma, Q. Yan, Surface Modified MXene-Based Nanocomposites for Electrochemical Energy Conversion and Storage. Small **15**, 1901503 (2019)
4. J. Calbo, M.J. Golomb, A. Walsh, Redox-active metal–organic frameworks for energy conversion and storage. J. Mater. Chem. A **7**, 16571–16597 (2019)
5. Y.F. Wang, H. Guo, X.D. Luo, X. Liu, Z.Z. Hu, L. Han, Z.Q. Zhang, Nonsiliceous Mesoporous Materials: Design and Applications in Energy Conversion and Storage. Small **15**, 1805277 (2019)
6. Y.J. Chen, A. Amiri, J.G. Boyd, M. Naraghi, Promising Trade-Offs Between Energy Storage and Load Bearing in Carbon Nanofibers as Structural Energy Storage Devices. Adv. Funct. Mater. **29**, 1901425–1901425 (2019)
7. Q.B. Yun, L.X. Li, Z.N. Hu, Q.P. Lu, B. Chen, H. Zhang, Layered Transition Metal Dichalcogenide-Based Nanomaterials for Electrochemical Energy Storage. Adv. Mater. **32**, 1903826 (2019)
8. J. Wang, Y. Cui, D. Wang, Design of Hollow Nanostructures for Energy Storage, Conversion and Production. Adv. Mater. **31**, 1801993 (2019)
9. G. Zhou, L. Xu, G.W. Hu, L.Q. Mai, Y. Cui, Nanowires for Electrochemical Energy Storage. Chem. Rev. **119**, 11042–11109 (2019)

10. E. Pomerantseva, F. Bonaccorso, X. Feng, Y. Cui, Y. Gogotsi, Energy storage: The future enabled by nanomaterials. Science **366**, 6468 (2019)
11. N. Devi, S. Sahoo, R. Kumar, R.K. Singh, A review of the microwave-assisted synthesis of carbon nanomaterials, metal oxides/hydroxides and their composites for energy storage applications. Nanoscale **13**, 11679–11711 (2021)
12. D.S. Bin, J. Lin, Y.G. Sun, Y.S. Xu, K. Zhang, A.M. Cao, L.J. Wan, Engineering Hollow Carbon Architecture for High-Performance K–Ion Battery Anode. J. Am. Chem. Soc. **140**, 7127–7134 (2018)
13. X.H. Lu, Y.X. Zeng, M.H. Yu, T. Zhai, C.L. Liang, S.L. Xie, M.S. Balogun, Y.X. Tong, Oxygen-Deficient Hematite Nanorods as High-Performance and Novel Negative Electrodes for Flexible Asymmetric Supercapacitors. Adv. Mater. **26**, 3148–3155 (2014)
14. A. Tang, C. Wan, X. Hu, X. Ju, Metal-organic framework-derived Ni/ZnO nano-sponges with delicate surface vacancies as anode materials for high-performance supercapacitors. Nano Res. **14**, 4063–4072 (2021)
15. K. Ren, Z. Liu, T. Wei, Z.J. Fan, Recent Developments of Transition Metal Compounds–Carbon Hybrid Electrodes for High Energy/Power Supercapacitors. Nano-Micro Lett **13**, 129 (2021)
16. Z. Zhang, X. Su, Y. Zhu, Z. Chen, Z. Fang, X. Luo, Porous multishelled NiO hollow microspheres encapsulated within three-dimensional graphene as flexible free-standing electrodes for high-performance supercapacitors. Nanoscale **11**, 16071–16079 (2019)
17. Q. Li, Y.H. Zhao, H.D. Liu, P.D. Xu, L.T. Yang, K. Pei, Q.W. Zeng, Y.Z. Feng, P. Wang, R.C. Che, Dandelion-like Mn/Ni Co-doped CoO/C Hollow Microspheres with Oxygen Vacancies for Advanced Lithium Storage. ACS Nano **13**, 11921–11934 (2019)
18. K.S. Ranjith, G.S.R. Raju, N.R. Chodankar, S.M. Ghoreishian, C.H. Kwak, S.H. Yun, Y.K. Han, Electroactive Ultra-Thin rGO-Enriched $FeMoO_4$ Nanotubes and MnO_2 Nanorods as Electrodes for High-Performance All-Solid-State Asymmetric Supercapacitors. Nanomaterials-basel **10**, 289 (2020)
19. Y. Jiao, C.C. Wan, Y.Q. Wu, J.Q. Han, W.H. Bao, H. Gao, Y.X. Wang, C.Y. Wang, J. Li, Ultra-high rate capability of nanoporous carbon network@V_2O_5 sub-micron brick composite as a novel cathode material for asymmetric supercapacitors. Nanoscale **12**, 23213–23224 (2020)
20. Y.D. Xue, Y.T. Wang, A review of the α-Fe_2O_3 (hematite) nanotube structure: recent advances in synthesis, characterization, and applications. Nanoscale **12**, 10912–10932 (2020)
21. J.Y. Ma, X.T. Guo, Y. Yan, H.G. Xue, H. Pang, FeO_x-Based Materials for Electrochemical Energy Storage. Adv. Sci. **5**, 1700986 (2018)
22. Y. Chen, C. Kang, L. Ma, L. Fu, G. Li, Q. Hu, Q. Liu, MOF-derived Fe_2O_3 decorated with MnO_2 nanosheet arrays as anode for high energy density hybrid supercapacitor. Chem. Eng. J. **417**, 129243 (2021)
23. Y. Lu, J.L. Qin, T. Shen, Y.F. Yu, K. Chen, Y.Z. Hu, J.N. Liang, M.X. Gong, J.J. Zhang, D.L. Wang (2021) Hypercrosslinked Polymerization Enabled N-Doped Carbon Confined Fe_2O_3 Facilitating Li Polysulfides Interface Conversion for Li–S Batteries. Adv. Energy Mater. 2101780

24. P.P. Yu, W. Duan, Y.F. Jiang (2020) Porous Fe_2O_3 Nanorods on Hierarchical Porous Biomass Carbon as Advanced Anode for High-Energy-Density Asymmetric Supercapacitors. Front. Chem., 2020, 8: 611852
25. C.Y. Zhou, X.C. Li, H.L. Jiang, Y. Ding, G.H. He, J. Guo, Z. Chu, G.H. Yu, Pulverizing Fe_2O_3 Nanoparticles for Developing Fe_3C/NCodoped Carbon Nanoboxes with Multiple Polysulfide Anchoring and Converting Activity in Li-S Batteries. Adv. Funct. Mater. **31**, 2011249 (2021)
26. S.T. Cheng, Y.X. Zhang, Y.P. Liu, Z.H. Sun, P. Cui, J.L. Zhang, X.H. Hua, Q. Su, J.C. Fu, E.Q. Xie, Energizing Fe_2O_3-based supercapacitors with tunable surface pseudocapacitance via physical spatial-confining strategy. Chem. Eng. J. **406**, 126875 (2021)
27. L.B. Wang, H.L. Yang, X.X. Liu, R. Zeng, M. Li, Y.H. Huang, X.L. Hu, Constructing Hierarchical Tectorum-like a-Fe_2O_3/PPy Nanoarrays on Carbon Cloth for Solid-State Asymmetric Supercapacitors. Angew. Chem. Int. Ed. **56**, 1105–1110 (2017)
28. P. Man, Q.C. Zhang, Z.Y. Zhou, M.X. Chen, J. Yang, Z. Wang, Z.X. Wang, B. He, Q.L. Li, W.B. Gong, W.B. Lu, Y.G. Yao, L. Wei, Engineering MoS_2 Nanosheets on Spindle-Like α-Fe_2O_3 as High-Performance Core–Shell Pseudocapacitive Anodes for Fiber-Shaped Aqueous Lithium-Ion Capacitors. Adv. Funct. Mater. **30**, 2003967 (2020)
29. Z.Y. Peng, J. Huang, Y. Wang, K. Yuan, L.C. Tan, Y.W. Chen, Construction of a hierarchical carbon coated Fe_3O_4 nanorod anode for 2.6 V aqueous asymmetric supercapacitors with ultrahigh energy density. J. Mater. Chem. A **7**, 27313–27322 (2019)
30. S.G. Dai, Y.C. Bai, W.X. Shen, S. Zhang, H. Hu, J.W. Fu, X.C. Wang, C.G. Hu, M.L. Liu, Core-shell structured Fe_2O_3@Fe_3C@C nanochains and Ni–Co carbonate hydroxide hybridized microspheres for high-performance battery-type supercapacitor. J. Power Sources **482**, 228915 (2021)
31. Z.M. Zheng, P. Li, J. Huang, H.D. Liu, Y. Zao, Z.L. Hu, L. Zhang, H.X. Chen, M.S. Wang, D.L. Peng, Zhang Q B, High performance columnar-like Fe_2O_3@carbon composite anode via yolk@shell structural design. J. Energy Chem. **41**, 126–134 (2020)
32. X. Wang, M. Zhang, E. Liu, F. He, C. Shi, C. He, J. Li, N. Zhao, Three-dimensional core-shell Fe_2O_3@carbon/carbon cloth as binder-free anode for the high-performance lithium-ion batteries. Appl. Surf. Sci. **390**, 350–356 (2016)
33. P.Y. Li, H.Y. Xie, X.Q. Wang, Y. Xie, Y.B. Wang, Y.K. Zhang, Sustainable production of nano α-Fe_2O_3/N-doped biochar hybrid nanosheets for supercapacitors. Sustain. Energ. Fuels **4**, 4522–4530 (2020)
34. R.R. Palem, S. Ramesh, H.M. Yadav, J.H. Kim, A. Sivasamy, H.S. Kim, J.H. Kim, S.H. Lee, T.J. Kang, Nanostructured Fe_2O_3@nitrogen-doped multiwalled nanotube/cellulose nanocrystal composite material electrodes for high-performance supercapacitor applications. J. Mater. Res. Technol. **9**, 7615–7627 (2020)
35. F. Han, J. Xu, J. Zhou, J. Tang, W. Tang, Oxygen vacancy-engineered Fe_2O_3 nanoarrays as free-standing electrodes for flexible asymmetric supercapacitors. Nanoscale **11**, 12477–12483 (2019)

36. S. Sun, T. Zhai, C.L. Liang, S.V. Savilov, H. Xia, Boosted crystalline/amorphous $Fe_2O_{3-\delta}$ core/shell heterostructure for flexible solid-state pseudocapacitors in large scale. Nano Energy **45**, 390–397 (2018)
37. S. Kumar, S. Telpande, V. Manikandan, P. Kumar, A. Misra, Novel electrode geometry for high performance CF/Fe_2O_3 based planar solid state micro-electrochemical capacitors. Nanoscale **12**, 19438 (2020)
38. J. Lia, Y.W. Wang, W.N. Xu, Y. Wang, B. Zhang, S. Luo, X.Y. Zhou, C.L. Zhang, X. Gu, C.G. Hu, Porous Fe_2O_3 nanospheres anchored on activated carbon cloth for high-performance symmetric supercapacitors. Nano Energy **57**, 379–387 (2019)
39. M. Zhou, B. Yang, Y.P. Zhao, Z.H. Jin, K. Li, L.P. Tang, Z.S. Cai, Facile preparation of N-doped carbon/FeO_x-decorated carbon cloth for flexible symmetric solid-state supercapacitors. Cellulose **27**, 1591–1601 (2020)
40. Y.W. Chen, Z. Guo, B.Q. Jian, C. Zheng, H.Y. Zhang, N-Doped Modified Graphene/Fe_2O_3 Nanocomposites as High-Performance Anode Material for Sodium Ion Storage. Nanomaterials-basel **9**, 1770 (2019)
41. A.C. Rodrigues, E.L.D. Silva, A.P.S. Oliveira, J.T. Matsushima, A. Cuña, J.S. Marcuzzo, E.S. Gonçalves, M.R. Baldan, High-performance supercapacitor electrode based on activated carbon fiber felt/iron oxides. Mater. Today Commun. **21**, 100553 (2019)
42. Y. Gu, W. Wen, S. Zheng, J. Wu, Rapid synthesis of high-areal-capacitance ultrathin hexagon Fe_2O_3 nanoplates on carbon cloth via a versatile molten salt method. Mater. Chem. Front. **4**, 2744–2753 (2020)
43. L. Wang, F. Liu, A. Pal, Y. Ning, W. Wu, Ultra-small Fe_3O_4 nanoparticles encapsulated in hollow porous carbon nanocapsules for high performance supercapacitors. Carbon **179**, 327–336 (2021)
44. P. Li, H.L. Wang, W.J. Fan, M.H. Huang, J. Shi, Z.C. Shi, S. Liu, Salt assisted fabrication of lignin-derived Fe, N, P, S codoped porous carbon as trifunctional catalyst for Zn-air batteries and water-splitting devices. Chem. Eng. J. **421**, 129704 (2021)
45. T. Zhou, Z.H. Shen, Y. Wu, T.L. Han, M.F. Zhu, X. Qiao, Y.J. Zhu, H.G. Zhang, J.Y. Liu, A yolk–shell Fe_3O_4@void@carbon nanochain as shuttle effect suppressive and volume-change accommodating sulfur host for long-life lithium–sulfur batteries. Nanoscale **13**, 7744–7750 (2021)
46. Q.C. Wu, R. Yu, Z.H. Zhou, H.W. Liu, R.L. Jiang, Encapsulation of a Core–Shell Porous Fe_3O_4@Carbon Material with Reduced Graphene Oxide for Li+ Battery Anodes with Long Cyclability. Langmuir **37**, 785–792 (2021)
47. Y.P. Huang, F. Cui, J. Bao, Y. Zhao, J.B. Lian, T.X. Liu, H.M. Li, $MnCo_2S_4$/$FeCo_2S_4$ “lollipop” arrays on a hollow N-doped carbon skeleton as flexible electrodes for hybrid supercapacitors. J. Mater. Chem. A **7**, 20778 (2019)

Figures

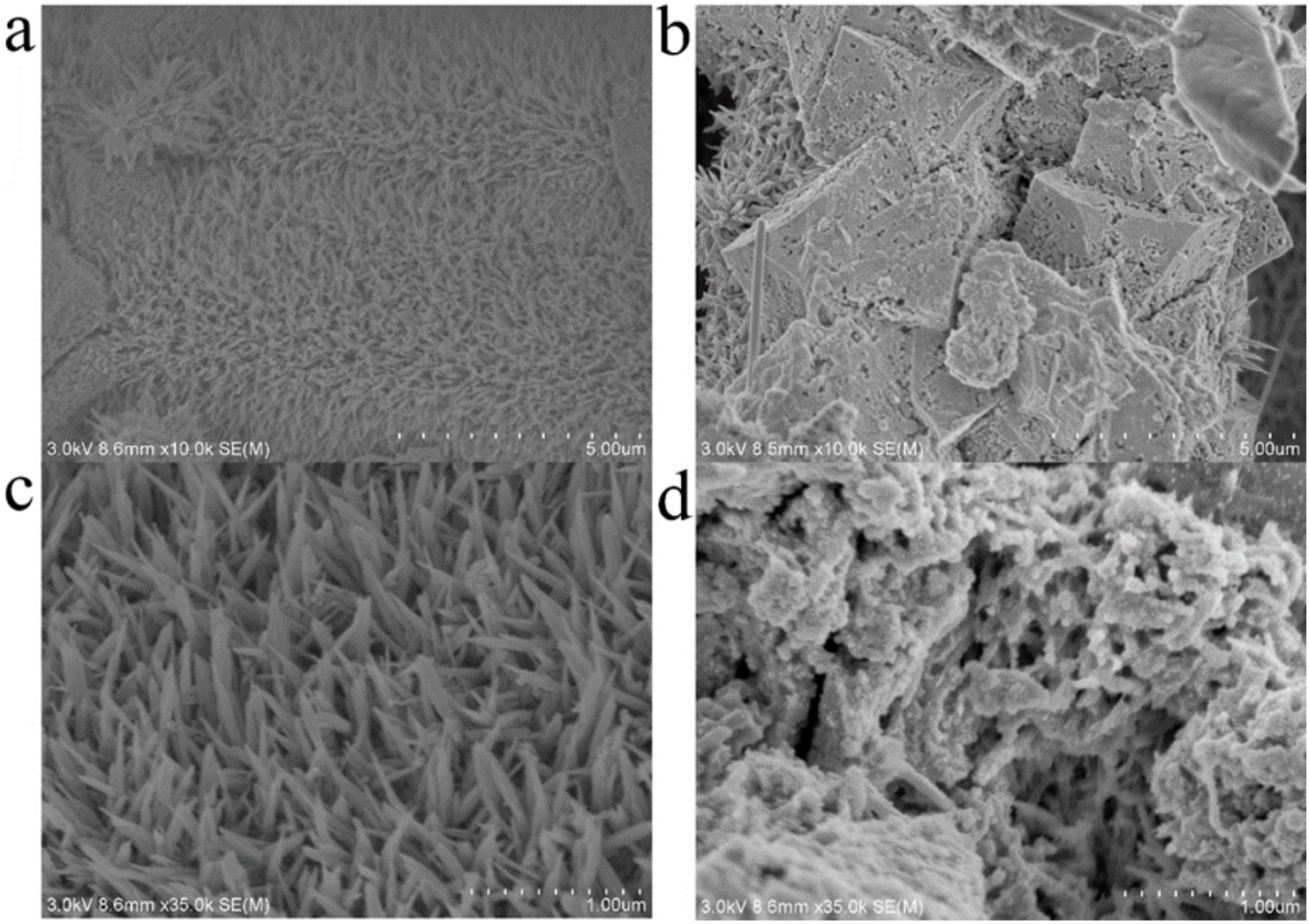

Figure 1

SEM images of (a,c) Fe2O3 and (b,d) Fe2O3/CN

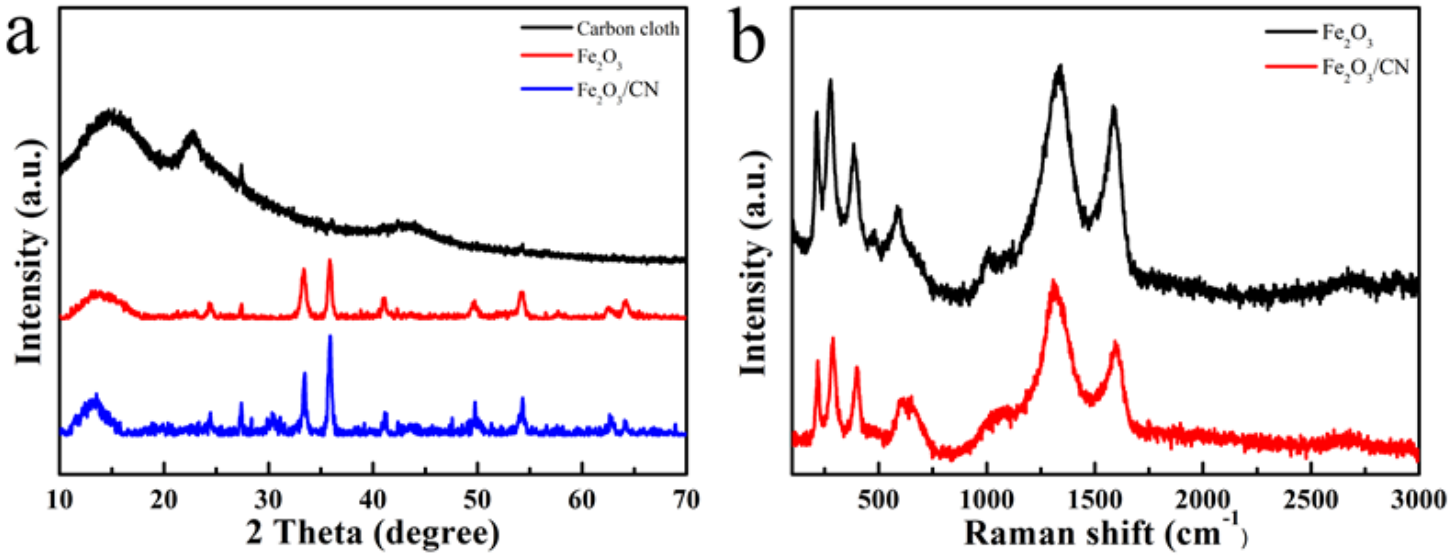

Figure 2

(a) X-ray diffraction (XRD) patterns and (b) Raman spectrum of Fe2O3 and Fe2O3/CN.

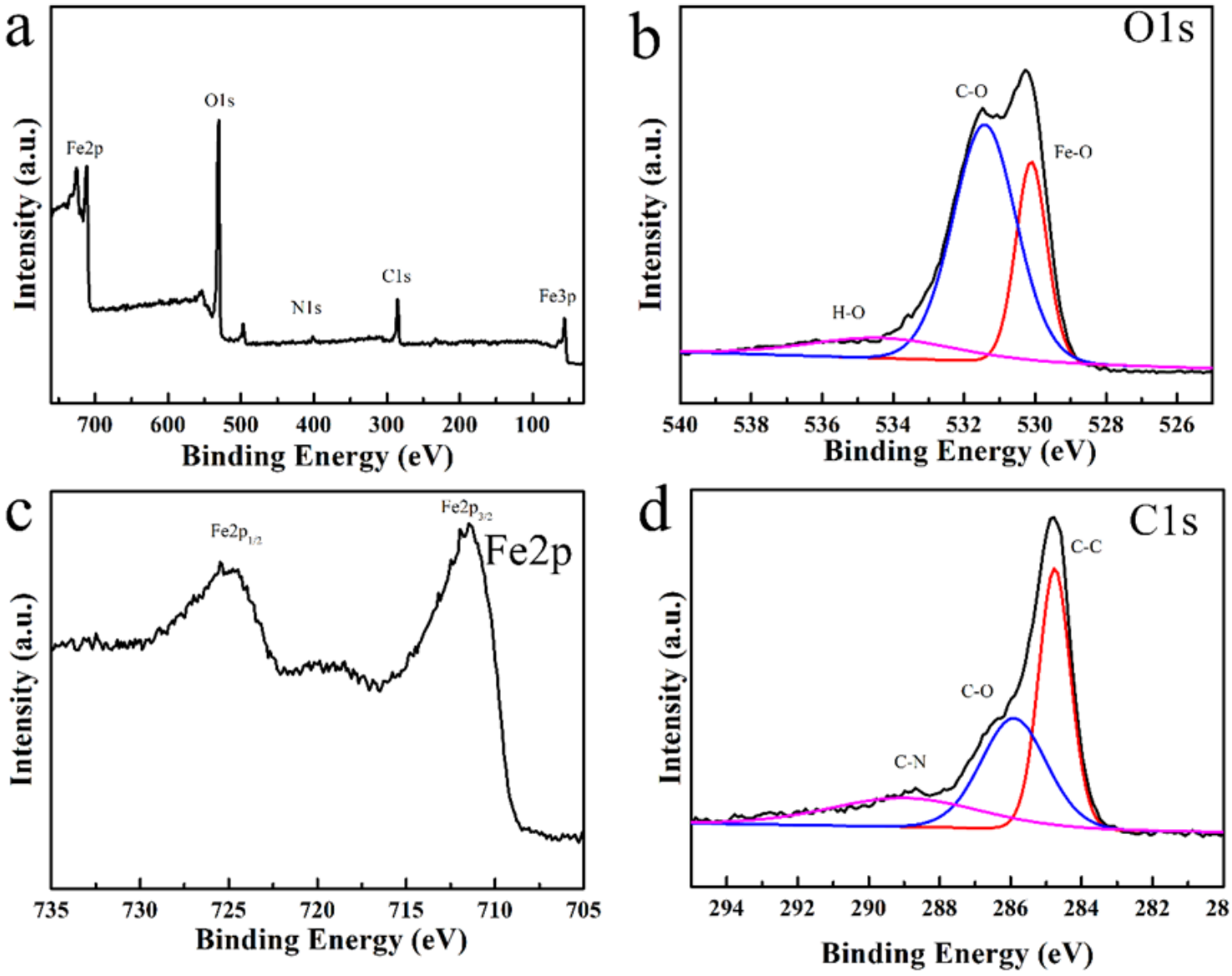

Figure 3

XPS spectra of Fe2O3/CN: (a) Survey scan, (b) O 1s, and (c) Fe 2p and (d) C 1s.

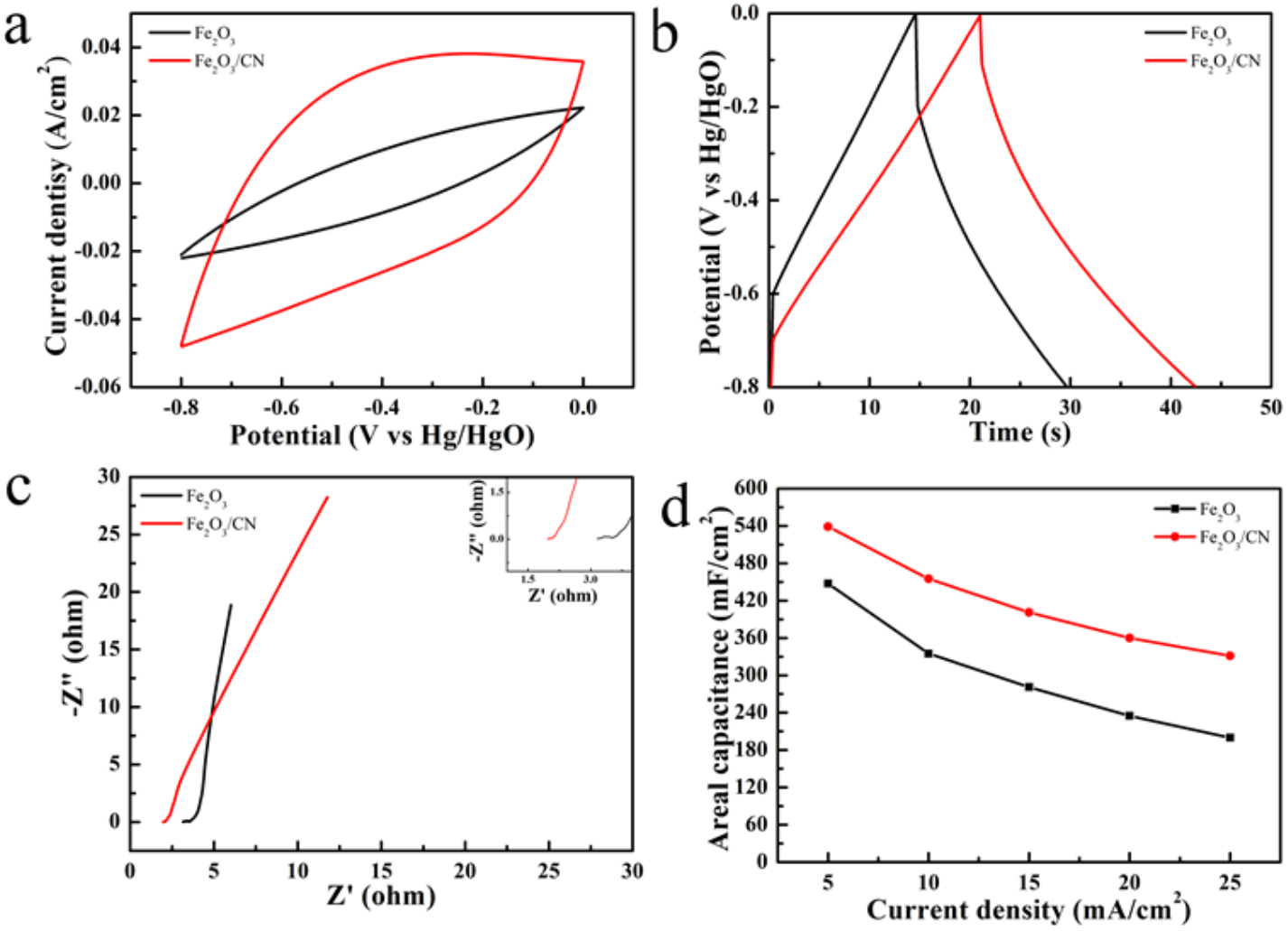

Figure 4

Electrochemical tests in the three-electrode system: (a) CV curves of Fe2O3 and Fe2O3/CN electrode at the scan rate of 100 mV/s; (b) charge–discharge curves at the current densities of 15 mA/cm2 for Fe2O3 and Fe2O3/CN electrode; (c) EIS of Fe2O3 and Fe2O3/CN electrode; (d) area specific capacitance for Fe2O3 and Fe2O3/CN electrode at different current.

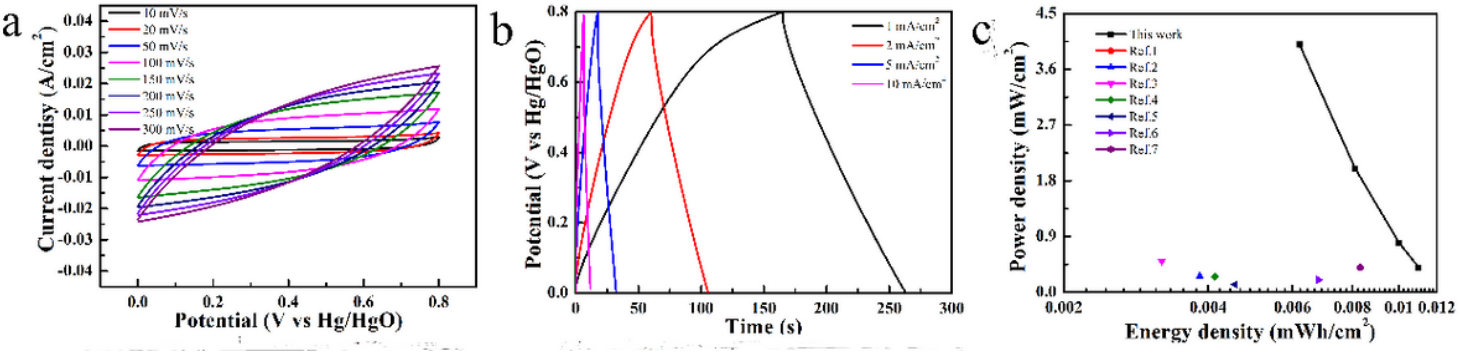

Figure 5

(a) CV curves of as-assembled symmetric supercapacitor device at different scan rates; (b) GCD curves of symmetric supercapacitor device at various current densities of the device; (c) ragone plots of the symmetric supercapacitor device.

Supplementary Files

This is a list of supplementary files associated with this preprint. Click to download.

- SupplementaryMaterials.docx
- Scheme1.png